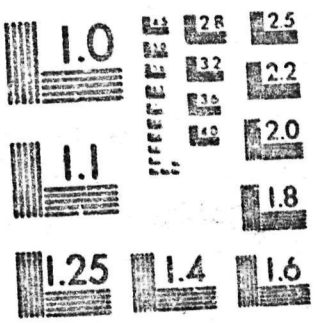

JPL PUBLICATION 78-41

(NASA-CR-157339) OPTIMAL SAMPLING AND QUANTIZATION OF SYNTHETIC APERTURE RADAR SIGNALS (Jet Propulsion Lab.) 43 p
HC A03/MF A01 CSCL 17I

N78-28301

Unclas
G3/32 27114

Optimal Sampling and Quantization of Synthetic Aperture Radar Signals

National Aeronautics and Space Administration

Jet Propulsion Laboratory
California Institute of Technology
Pasadena, California

JPL PUBLICATION 78-41

Optimal Sampling and Quantization of Synthetic Aperture Radar Signals

Chialin Wu

June 15, 1978

National Aeronautics and
Space Administration

Jet Propulsion Laboratory
California Institute of Technology
Pasadena, California

The research described in this publication was carried out by the Jet Propulsion Laboratory, California Institute of Technology, under NASA Contract No. NAS7-100.

PREFACE

The work described in this report was performed by the Information Systems Division of the Jet Propulsion Laboratory.

ABSTRACT

This paper presents some theoretical and experimental results on optimal sampling and quantization of synthetic aperture radar (SAR) signals. It includes a description of a derived theoretical relationship between the pixel signal-to-noise ratio of processed SAR images and the number of quantization bits per sampled signal, assuming homogeneous extended targets. With this relationship known, a solution may be realized for the problem of optimal allocation of a fixed data bit-volume (for specified surface area and resolution criterion) between the number of samples and the number of bits-per-sample. The results indicate that to achieve the best possible image quality for a fixed bit rate and a given resolution criterion, one should quantize individual samples coarsely and thereby maximize the number of multiple looks. The theoretical results are then compared with simulation results obtained by processing aircraft SAR data.

CONTENTS

PRINTS (contd)

I. INTRODUCTION

The high data rate and data volume associated with a synthetic aperture radar (SAR)[1],[2] present a problem in designing a SAR for use onboard a spacecraft because the data transmission rate and data storage capacity are usually limited for various practical reasons. SAR data rate and data volume are also a problem in the design of a SAR signal processing system because it requires a tradeoff between the hardware complexity--which is generally related to the memory capacity, processing speed, etc.--and the quality of the output product.

Many people [3], [4] have suggested azimuth prefiltering to reduce the SAR data rate. This approach is based on the fact that the azimuth bandwidth is often greater than that necessary to satisfy spatial resolution requirements. The required number of data samples is reduced by reducing the effective azimuth bandwidth, but it has not been clear how to perform azimuth prefiltering in an optimal manner. For example, it is well known that "excess" azimuth bandwidth (if not removed by prefiltering) can be used to reduce communication and "speckle" noise. The tradeoff in an analog signal transmission system with transmission power fixed can be between increasing the signal bandwidth versus increasing the receiver input signal-to-noise ratio. In a digital system with a constraint on the number of data bits per total image, the tradeoff can be between increasing the total number of azimuth samples versus finer quantization of each signal sample.

To achieve optimality, one requires a thorough understanding of the characteristics of SAR images and the effects of noise, limiting and other factors on the output image quality. Work toward this objective has been reported in the SAR processing area [5] - [7]. Related work, [8] - [10] can

also be found in the area of holographic processing. Generally speaking, the references treat a limited aspect of the problem. This paper reports on an effort to develop a unified treatment of a broader range of factors. Detailed analysis as well as simulations were conducted. Major emphasis was placed on the digital aspects of the SAR data system. The results are useful in the design of optimal SAR data processing systems and provide a better understanding of how different factors affect SAR image characteristics.

Section II of this paper contains an analysis of the performance of a SAR image processor. A model of extended and Rayleigh distributed targets is assumed. The signal-to-noise ratio of a SAR processor output is then calculated. In Section III, the effect of signal quantization as related to the processor output signal-to-noise ratio is discussed. In the extreme case of one-bit quantization, two approaches to compute the signal-to-noise ratio are used. One approach is to assume quantization noise is random and additive; and the other approach is to assume the input signal is hard limited. Both approaches yield nearly the same results. In cases involving more than one quantization bit, the former approach is utilized.

Simulation results are reported in Section IV. Some discussion related to the evaluation of image quality is also included. Finally, Section V contains a discussion of the significance of this study.

II. THE PERFORMANCE OF A SAR DATA PROCESSOR

In this section, we analyze the output pixel signal-to-noise ratio, which is chosen as the primary index for measuring the SAR image quality. The inputs to the processor are the received SAR echoes (contaminated by noise) in the form of baseband inphase and quadrature signals. The processor is assumed to be an ideal processor where the input signals are correlated

with a complex reference function, namely, the complex conjugate of the response of a point target with unit reflectance. The processor output comprises both the true image signals and noise. In this context, the noise in the output image includes contributions resulting from additive noise in the received SAR echo and artifacts, e.g., integrated sidelobes, resulting from signal compression.

II.1 Model of Extended Targets

A distinctive feature of the model is that the target area corresponding to resolution cell is not assumed to be a surface exhibiting uniform isotropic reflectance. Instead, it is assumed that in each cell there are a finite number of "scattering centers" randomly located in that area. (Individual scattering centers are assumed to reflect incident illumination in an isotropic manner.) Because these scattering centers are randomly located, the apparent reflectance of a cell in response to monochromatic illumination can be quite varied. At a specific vantage point, the monochromatic illumination reflected by the individual scattering centers within a resolution cell may add in a constructive or destructive manner depending on geometric factors. In other words, the resolution cell exhibits wavelength-dependent peculiarity which is a function of the fine structure interval of the cell. In practical SAR system (having finite size synthetic apertures), the varied scattering pattern within resolution cells will result in differences in the sensed energy in the reflected signal from individual cells though the total energy reflected by each cell may be the same. Therefore, the sensed "brightness" of a resolution cell in a radar image is not exactly proportional to the total energy reflected by that cell. This random fluctuation of brightness,

which is a general characteristic of SAR and laser images, is often referred to as "speckles."[11]-[13] Images obtained with broad spectrum illumination do not exhibit speckles because the "speckles" associated with specific wavelengths tend to average out.

A mathematical modeling of the reflective coefficient $\sigma(x,r)$--whose derivation is based on the assumption that the number of scattering centers is sufficiently large such that the central limit theorem can be applied--of a resolution cell located at coordinate (x,r) imaged by a SAR can be written as follows:

$$\sigma(x,r) = \sigma_0(x,r) \cdot \gamma \cdot \exp(j\phi) \qquad (1)$$

where $\sigma_0(x,r)$ represents the mean amplitude reflectance of a cell averaged over all observation angles and is real and positive.

γ is a random variable of the Rayleigh distribution

ϕ is a random phase factor uniformly distributed over 2π radians in $(0,2\pi)$

x specifies the position of a resolution cell along the line of flight of the SAR, i.e., the azimuth direction

and r specifies the slant range from the radar to the resolution cell.

Eq. 1 is a widely accepted[11],[12] model of the radar image elements obtained from the observation of a rough surface. Note that Eq. 1 is defined over the entire region of (x,r) of interest. We will further assume that the true reflectance $\sigma_0(x,r)$ is "homogeneous" in the region surveyed.

The assumption of homogeneous targets is reasonable if the area being imaged does not exhibit a large change of reflectance characteristics in different regions of the target area, such that the mean echo power is nearly constant. This is very important in analyzing the effect of hard-limiting due to insufficient dynamic range in a SAR data system. And the limiting may cause significant "weak signal suppression" in regions where the assumption of homogeneous targets does not apply.

By performing quadrature detection processing (as discussed in the next subsection), one can eliminate the effects of the random phase factor $\exp(j\phi)$ of Eq. 1. However, one would have to process an infinite amount of data, i.e., infinite looks, to totally suppress the random amplitude factor γ. In practice this leads to a trade-off between image quality and spatial resolution. The factor γ manifests itself as seemingly random variations in the intensity of elements of the radar image. This type of image "distortion" was referred to as "speckles" in a previous section.

A few statistical properties of the scattering coefficient $\sigma(x,r)$ are given here. The subscript "i" is used to denote a cell at (x_i,r_i). Eq. 1 may be expressed as:

$$\sigma_i = \sigma_i^I + j\sigma_i^Q \tag{2}$$

with

$$\sigma_i^I = \sigma_{io}\,\gamma_i \cos\phi_i \tag{3a}$$

$$\sigma_i^Q = \sigma_{io}\,\gamma_i \sin\phi_i \tag{3b}$$

γ_i and ϕ_i are random variables as defined in Eq. 1. The superscripts I and Q represent inphase and quadrature components (or the real and imaginary

parts) of σ_i, respectively. Eq. 3a and 3b are intermediate steps in deriving expression (1). The factors $(\gamma_i \cos \phi_i)$ and $(\gamma_i \sin \phi_i)$ are independent identically distributed random variables from a normal density function with zero mean and unit variance, i.e.,

$$\gamma_i \cos \phi_i,\ \gamma_i \sin \phi_i \sim N(0,1) \tag{4}$$

For later use, we define the amplitude of reflectance, A_i, as

$$A_i = \sigma_{io}\, \gamma_i \tag{5}$$

The power P_i, received from a cell i is

$$P_i = |\sigma_i|^2 = \sigma_{io}^2\, \gamma_i^2 = A_i^2 \tag{6}$$

The mean signal power, P, averaged over the ensemble of all i's is

$$P = \langle P_i \rangle = \langle A_i^2 \rangle = \langle \sigma_{io}^2 \rangle \langle \gamma_i^2 \rangle = 2 \langle \sigma_{io}^2 \rangle = 1 \tag{7}$$

where a pair of brackets, $\langle \cdot \rangle$, denotes the mean or expected value of the quantity in the brackets. Also note that the mean power has been arbitrarily normalized for computational convenience.

II.2 Signal Processor

The pulse repetition rate of a SAR is such that a point target on the surface is "interrogated" many times as it passes through the azimuth beamwidth of the radar antenna. The elapsed time between the transmission of a pulse and the receipt of the corresponding echo is a measure of the range from radar to the target. The ensemble of echo signals can be assembled into a rectangular display with elapsed time (range, r) along one axis and azimuth position (x) along the other axis. The idealized receiver output--is at

baseband, and it contains both inphase and quadrature components. The time reference is expressed in terms of the corresponding spatial coordinates (x,r). With these conditions, the receiver output corresponding to an isolated unit target located at (x_o, r_o) can be represented as follows:

$$h(x-x_o, r-r_o, r_o) = \begin{cases} a(r_o)\exp[-j\frac{2\pi}{\lambda r_o}(x-x_o)^2 + j\frac{2b}{c}(r-r_o)^2] & \text{for } (x-x_o, r-r_o) \in R \\ 0 & \text{otherwise} \end{cases} \quad (8)$$

where $a(r_o)$ represents attenuation due to radar path loss to a target at range r_o

λ = the wavelength of the transmitted EM wave,

b = the FM chirp rate of the transmitted pulse,

c = the speed of light,

and R = the region of responsiveness determined by the antenna azimuth beamwidth and the duration of the transmitted pulse.

Notice that we have assumed that linear FM chirp pulses are transmitted. It is also assumed that geometric factors justify the approximation that the range of the target, r_o, is constant as the target passes through the azimuth beamwidth.

For a continuous reflective surface, the received signal is a superposition of the contributions from all the targets within the antenna beam. The contribution from each target is a function of its reflectance, $\sigma(x, r)$ in Eq. 1, and the impulse response defined in Eq. 8. The receiver output also contains additive noise. The net output, f(x, r), may be expressed as:

$$f(x, r) = n + \iint \sigma(x', r') h\,(x - x', r - r', r')\, dx'\, dr' \qquad (9)$$

where n is a random variable denoting the additive noise in the signal. Equation 9 represents a convolution process. A correlator with a reference function $h^*\,(x - x', r - r', r')$, the complex conjugate of h in Eq. 8, can be used to reconstruct a scene $|\hat{\sigma}\,(x, r)|^2$ which is an estimation of the intensity of the complex reflectance denoted by $\sigma_o^2\,(x, r)\cdot\gamma^2$ or A_1^2 in the previous subsection.

A block diagram of a SAR correlator which employs the quadrature detection algorithm is shown in Fig. 1. The input comprises the received echoes, and the output is an estimation of $|\sigma(x, r)|^2$. The details of implementing such a correlator in the form of an optical or electronic processor is not within the scope of this study. We therefore confine our discussion to a theoretical analysis of the performance of the correlation processor.

II.3 Signal-to-Noise Ratio of the Processor Output

The criteria for evaluating SAR image quality have not been fully developed to date. Some recent work related to this particular problem is reported in Ref. [6] [14]. In this study, the processor output signal-to-noise ratio is used as the criterion to evaluate the processed SAR images. The signal component of an output image element is defined to be a normalized measure of the expected target intensity reflectance. Any difference between this signal component and the actual output is regarded as noise. Thus defined noise includes distortions resulting from all factors. Primary

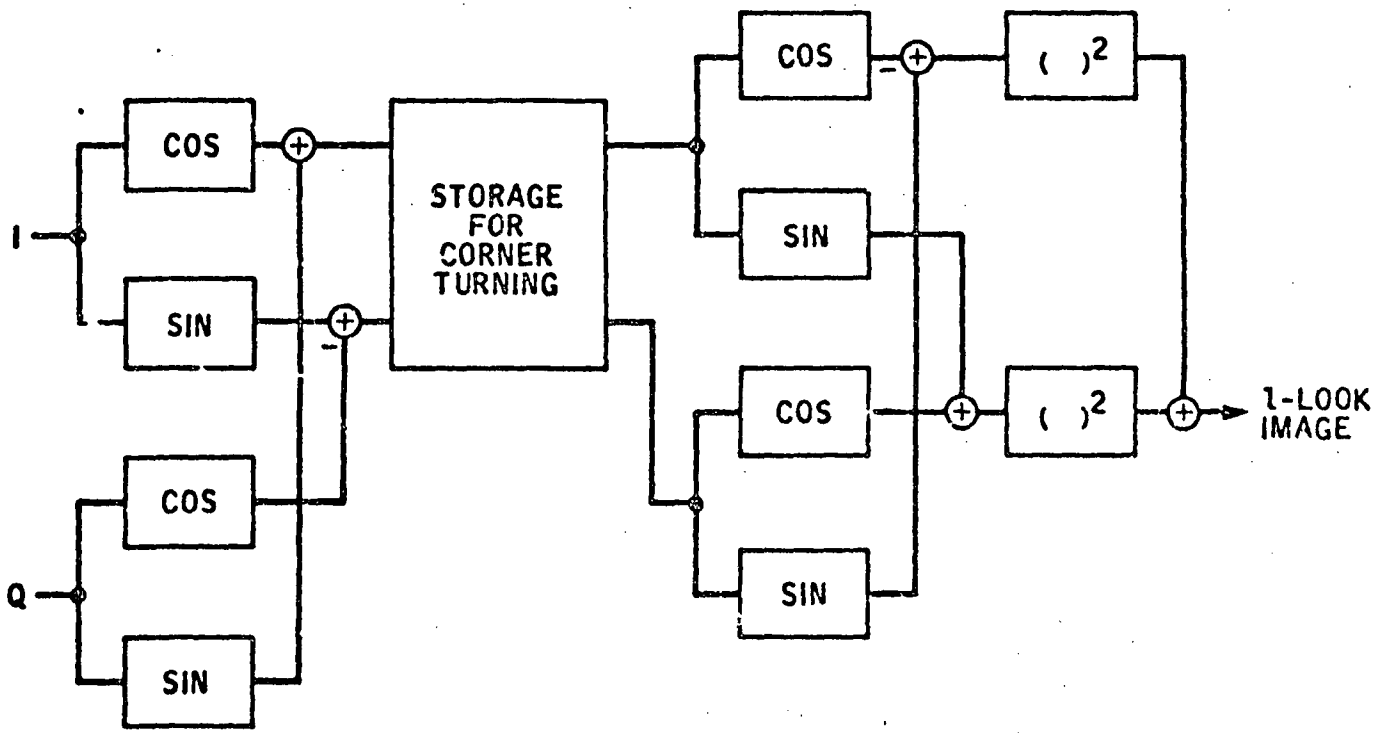

Figure 1 Block Diagram for Processing SAR Data Into Images

causes of distortion in practical systems include thermal noise, spurious echoes in antenna sidelobes, quantization errors, pulse compression integrated sidelobes, and speckles. With "noise" being defined in this manner, the output image element signal-to-noise ratio can serve as a very effective measure of the quality of SAR images.

The analysis is based on the SAR signal model discussed in the previous subsection. The idealized receiver output when it is written in discrete form becomes

$$f(i,k) = n_{i,k} + \sum_{l=-N/2}^{N/2} \sum_{m=-M/2}^{M/2} A_{i+l,k+m} \exp \gamma \left[\alpha_r l^2 + \beta m^2 + \phi_{i+l,k+m}\right] \quad (10)$$

where i and k are indices of discrete signal samples

l and m denote increments from indices i and k

n_{ik} is the noise in signal sample $f(i,k)$.

$A_{i+e,k+m}$ is the target amplitude reflectance as defined in Eq. 5.

N and M are the azimuth and range compression ratios (time-bandwidth products) respectively.

α_r and β are frequency sweep parameters of the azimuth and range chirps, respectively.

$\phi_{i+l,k+m}$ is the random phase factor as defined in Eq. 1.

In Eq. 10, a subscript "r" is used in the azimuth frequency sweep parameter α_r to denote that α_r is range dependent.

To reconstruct an image point at position (0,0), two-dimensional range and azimuth correlation is required. The reference function for correlation can be written as:

$$g(i,k) = \exp - \gamma\left[\alpha_r i^2 + \beta k^2\right] \qquad |i| \le \frac{N}{2} \; |k| \le \frac{M}{2} \tag{11}$$

The correlation of $f(i,k)$ and $g(i,k)$ as denoted by X_0 can be expressed as follows:

$$X_0 = \sum_{i=-N/2}^{N/2} \sum_{k=-M/2}^{M/2} f(i,k) \cdot g(i,k)$$

$$= \sum_{i=-N/2}^{N/2} \sum_{k=-M/2}^{M/2} \left\{ n_{i,k} \exp - \gamma[\alpha_r i^2 + \beta m^2] \right.$$

$$\left. + \sum_{l=-N/2}^{N/2} \sum_{m=-M/2}^{M/2} A_{i+l,k+m} \exp \gamma[\alpha_r (l^2 - i^2) + \beta(m^2 - k^2) + \phi_{i+l,k+} \right. \tag{12}$$

By properly changing the indices of summations and rearranging their orders we have:

$$X_0 = S_0 + N_0 + N_b \tag{13}$$

where $$S_0 = (N + 1)(M + 1) A_{0,0} \exp(\gamma \phi_{0,0}) \tag{14}$$

$$N_0 = \sum_{i=-N/2}^{N/2} \sum_{k=-M/2}^{M/2} n_{i,k} \exp -\gamma[\alpha_r i^2 + \beta k^2] \tag{15}$$

$$N_b = \sum_{\substack{l=-N \\ l \neq 0}}^{N} \sum_{\substack{k=-M \\ k \neq 0}}^{M} A_{i,k} \exp(\gamma \phi_{i,k}) \cdot b_{i,k} \tag{16}$$

$$b_{i,k} = \sum_{l=-\frac{N}{2}+i}^{N/2} \sum_{m=-\frac{M}{2}+k}^{M/2} \exp \gamma\left\{\alpha_r\left[(1-i)^2 - l^2\right] + \beta\left[(m-k)^2 - k^2\right]\right\} \tag{17}$$

The physical meaning of S_o, N_o, and N_b are the true signal component, the noise component due to input noise, and the noise component due to integrated sidelobes respectively. The term $b_{i,k}$ is the i,k-th sidelobe resulting from auto-correlation of the chirp g of Eq. 11. Since the random quantities $\{n_{i,k}\}$ and $\{\phi_{i,k}\}$ are all mutually independent, the mean energy of X_o is

$$P_X = \langle |X_o|^2 \rangle = P_S + P_N \tag{18}$$

where $$P_S = N^2M^2 \langle A_{o,o}^2 \rangle \tag{19}$$

$$P_n = NM\langle n_{i,k}^2 \rangle + \sum_{\substack{i=-N \\ i\neq 0}}^{N} \sum_{\substack{k=-M \\ k\neq 0}}^{M} \langle A_{i,k}^2 \rangle \, | \, b_{i,k} | \, ^2 \tag{20}$$

P_s and P_n represent the mean energy of signal and noise, respectively. Eq. 20 is arrived at by assuming that $n_{i,k}$ is a two dimensional white Gaussian noise. Also note that we have replaced the product of (N + 1) (M + 1) by NM in Eqs. 19 and 20 for simplicity. The mean of $A_{i,k}^2$ is normalized to be unity according to Eq. 7. The mean of $n_{i,k}^2$ is σ_n^2, by assuming the Gaussian noise statistics

$$n_{i,k}^{I,Q} \sim N(0, \sigma_n^2/2) \tag{21}$$

And the summation in P_n is evaluated as $0.2N^2M^2$, where the factor 0.2 is the approximated value obtained by numerical integration of the energies in the sidelobes produced by compression of the two-dimensional linear FM chirp. The quantities related to mean energy thus become

$$P_S = N^2M^2 \tag{22}$$

$$P_n \cong NM\,\sigma_n^2 + 0.2\,N^2M^2 \tag{23}$$

$$\text{and}\quad P_x \cong NM\,\sigma_n^2 + 1.2\,N^2M^2 \tag{24}$$

The definition for output signal-to-noise ratio used in Ref. [5], $(SNR)_o$, will also be used here. It is defined as the ratio of mean signal energy to the standard deviation of the processor detector output $|X_o|^2$. That is

$$(SNR)_o = \frac{P_s}{V_x} \tag{25}$$

According to Eqs. 13-17, X_o forms a two dimensional Gaussian process for homogeneous targets. The detector output $v = |X_o|^2$ thus forms an exponential distribution with pdf $f(v) = (1/P_x)\exp(-v/P_x)$. Since the mean and standard deviation of an exponentially distributed random variable are equal, the output signal-to-noise ratio now becomes

$$(SNR)_o = \frac{P_s}{P_x} \tag{26}$$

$$= \frac{1}{\frac{\sigma_n^2}{NM} + 1.2}$$

The above expression can also be written in terms of the input signal-to-noise ratio, $(SNR)_i$. The received signal is given by Eq. 10, of which $n_{i,k}$ is the input noise component, and the summation is the input signal component. With $n_{i,k}$ and $\{\phi_{i,k}\}$ being independent, the mean energy of $f(i,k)$ is easily evaluated, i.e.,

$$\langle |f|^2 \rangle = \sigma_n^2 + NM \tag{27}$$

The input signal-to-noise ratio, $(SNR)_i$, is

$$(SNR)_i = \frac{NM}{\sigma_n^2} \tag{28}$$

We can now rewrite $(SNR)_o$ as

$$(SNR)_o = \frac{1}{(SNR)_i^{-1} + 1.2} \tag{29}$$

From the above expression it is observed that contributions due to integrated sidelobes and speckles can be limiting factors in the performance of an SAR processor. Although sidelobe suppression can be achieved by spectrum weighting [15][16], the tradeoff is a higher computation load in a digital SAR processor in order to preserve original image resolution.

III. EFFECTS OF QUANTIZATION AND MULTIPLE-LOOK

In this section the effects of input signal quantization and image post-detection multiple-look are treated. With these two effects known, the problem of how to optimally sample and quantize SAR signals is readily solved.

III.1. Effect of Quantization

A common approach to investigate the effect of quantization is by modeling quantization error with random additive noise. We assume that the in-phase and quadrature components of the received signal f(i,k) are separately quantized, and the quantization error n_q is zero mean, additive, and independent of the original signal and noise as given in Eq. 10. Also we assume the statistics of quantization error n_q^I, n_q^Q to be

$$\langle n_q^I \rangle = \langle n_q^Q \rangle = 0 \tag{30a}$$

$$\langle (n_q^I)^2 \rangle = \langle (n_q^Q)^2 \rangle = \frac{\sigma_q^2}{2} \tag{30b}$$

Further, we assume that the quantizer is optimally designed. Because the SAR signals are known to form a two dimensional Gaussian process for homogeneous targets, the amount of quantization error, σ_q^2, can be directly related to the number of quantization levels and the signal energy. That is

$$\sigma_q^2 = \langle n_q^{I2} \rangle + \langle n_q^{Q2} \rangle = e \cdot \frac{\langle |f|^2 \rangle}{2} + e \cdot \frac{\langle |f|^2 \rangle}{2} = e \langle |f|^2 \rangle \tag{31}$$

where e is a parameter dependent upon the number of quantization levels. The values of e for the minimum distortion quantization were tabulated in Ref. [17]. The expression for the signal energy $|f|^2$ appears in Eq. 27. Eq. 31 therefore is

$$\sigma_q^2 = e\,(\sigma_n^2 + NM) \tag{32}$$

By treating the quantization error as an independent source of input noise, Eq. 26 can be rewritten as

$$(SNR)_o = \frac{1}{\frac{\sigma_n^2 + \sigma_q^2}{NM} + 1.2} \tag{33}$$

Substituting Eq. 32 into above, and making use of the input SNR defined in Eq. 28, the output pixel $(SNR)_o$ which includes the effect of input sample quantization error becomes

$$(SNR)_o = \frac{1}{(1 + e)\ (SNR)_i^{-1} + (1.2 + e)} \tag{34}$$

III.2. Effect of Hard-Limiting

Note that one bit quantization corresponds to the "hard limiting" of the SAR receiver output bipolar signals. Since such limiting is a non-linear process, it is questionable whether the model of additive white noise for quantization error (used in the foregoing discussion) is still valid. We now treat the case of signal limiting. The result can be used to verify the results derived in the previous subsection for the case of one bit per sample. A detailed treatment of the effect of hard limiting is given in Ref. [18]. Some related results are briefly discussed here.

The resultant mean output signal power (with input signal being hard limited in both inphase and quadrature channels) for homogeneous targets and large compression ratio can be written as follows:

$$P_s = \langle |S_o|^2 \rangle \simeq \frac{2}{\pi} N^2 M^2 \langle A_{o,o}^2 \rangle = \frac{2}{\pi} N^2 M^2 \tag{35}$$

where we have assumed that the hard limited input amplitude is normalized such that the mean input energy ($\langle |f|^2 \rangle$ of Eq. 27) is unchanged. The mean correlation output energy, R, is

$$R = NM\ [\sigma_n^2 + NM] \tag{36}$$

The output pixel SNR as defined in Eqs. 25 and 26 becomes

$$(SNR_b)_o = \frac{P_s}{R}$$

$$\simeq \frac{2}{\pi} \frac{1}{\frac{\sigma_n^2}{NM} + 1}$$

$$= \frac{2}{\pi} \frac{1}{(SNR)_i^{-1} + 1} \qquad (37)$$

The subscript "b" denotes binary input signal sample. It is noted that a possible -1.9 db degradation in output pixel SNR may be encountered for homogeneous targets return as compared to Eq. 29 which applies to the case involving processing of a linear (unquantized) input signal. Indeed the expressions of Eqs. 29 and 37 represent the two extreme cases for signal quantization, and therefore can serve as performance bounds in studying the effect of input quantization. A plot of Eqs. 29 and 37 is shown in Fig. 2, where the $(SNR)_o$ is plotted versus the $(SNR)_i$ values. Results derived from Eqs. 29 and 37 are joined by solid lines. And the points joined by dashed lines are derived from Eq. 34 for the two cases of 1 and 2 quantization bits per I and Q input sample. From these curves, it is observed that at low $(SNR)_i$, i.e., the left portion of the graph, the output $(SNR)_o$ increases approximately linearly with the increase of $(SNR)_i$. And the output $(SNR)_o$ saturates for high input $(SNR)_i$ due to the effects of speckles and integrated sidelobes, since their magnitudes are generally proportional to the signal power. The two curves for one-bit quantization, which were derived using two different approaches, are indeed very close to each other. This enhances our confidence in the validity of the analytical results.

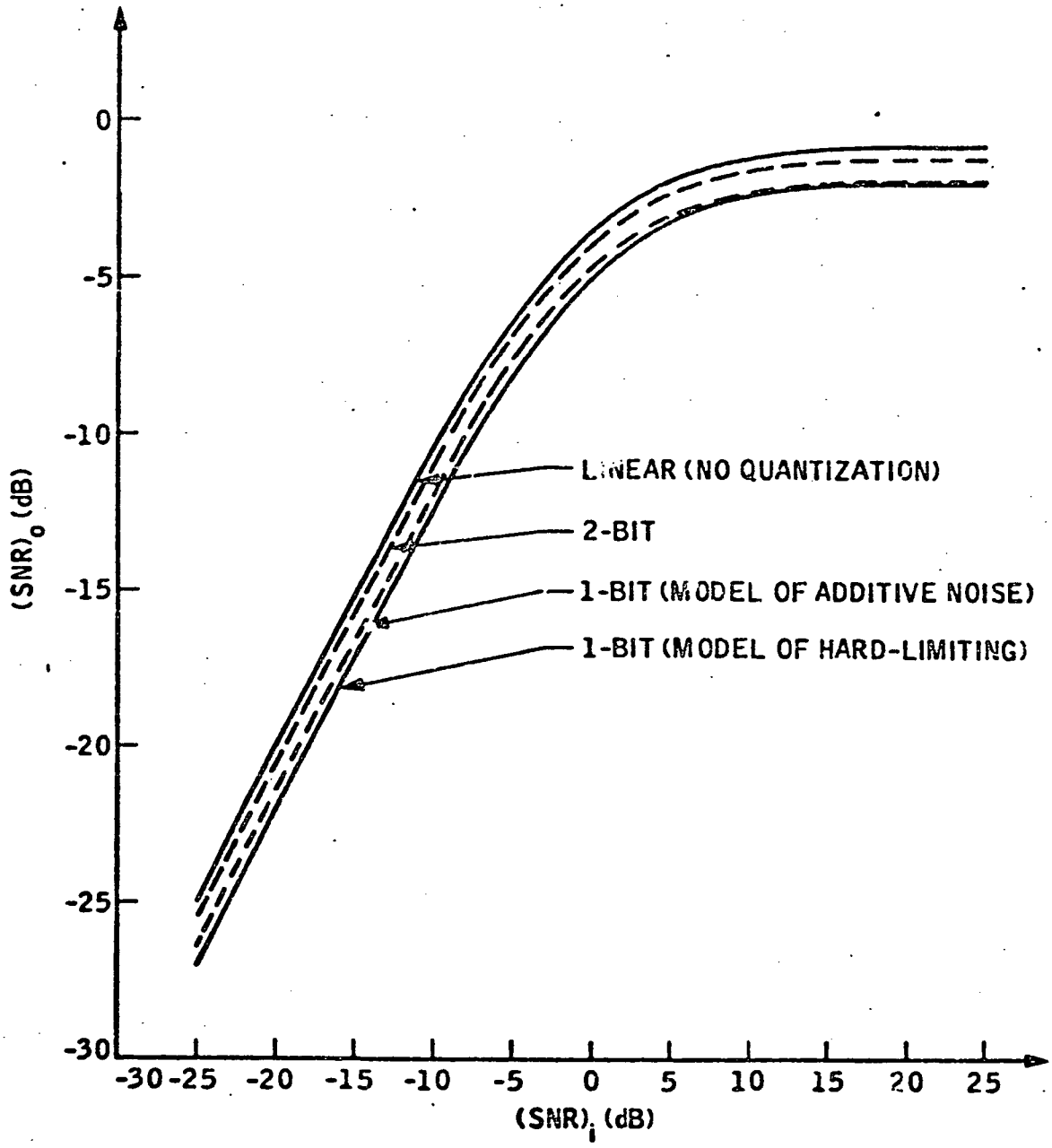

Figure 2 Output $(SNR)_o$ versus Input $(SNR)_i$ for single-look SAR Images with Different Input Quantization Bits

III.3 Effect of Multiple Look

Since the quality of SAR images is degraded by speckles, it is desirable to perform the "post-detection integration" to suppress this type of noise. The post-detection integration involves averaging of independent image resolution elements, therefore, this process is often called "multiple-look." We now define that a L-look image is obtained by averaging L independent image pixels which correspond to the same resolution and location. The averaging process does not alter the mean of the pixel energy but simply reduces the standard deviation of the pixel variation to $(\sqrt{L})^{-1}$ of its one-look value. Therefore, according to the definition of $(SNR)_0$ discussed in Eqs. 25 and 26, it is known [5] that

$$(SNR)_L = \sqrt{L}\,(SNR)_0 \qquad L \geq 1 \tag{38a}$$

and

$$(SNR_b)_L = \sqrt{L}\,(SNR_b)_0 \qquad L \geq 1 \tag{38b}$$

where the subscript "L" denotes L-look images. From this equation, it is noted that L-look processing may enhance the quality of a single-look image by a factor of $\sqrt{L}$.

III.4. Optimal Use of a Limited Bit Rate

It is sometimes required to digitally represent the sampled output of a SAR receiver in a manner which tends to maximize the image quality without exceeding a specified data rate. It is assumed here that the spatial resolution is specified and that "data compression" will not be used. The data rate will therefore equal the product of the SAR signal sampling rate times the number of bits per sample. One must therefore optimally balance a trade-off of sampling rate versus fineness of sample quantization. The signal-to-

noise ratio in the output image (in the sense described in Section III.3) will be used as the measure of image quality.

To simplify the discussion, we assume that the input signal-to-noise ratio is independent of sampling rate. This assumption is valid if the signal and noise spectra in the region of interest are sufficiently flat that prefiltering (to avoid aliasing at reduced sampling rates) does not cause a significant change in the input signal-to-noise ratio. Results derived from Eq. 34 and 38a are plotted in Figure 3, where the $(SNR)_o$ versus the number of quantization bits, N_B, is plotted. All the points in this figure correspond to the same input data bit - rate (or volume) output image area, and spatial resolution. This can be represented by a constant product of input quantization bits, N_B, and number of "looks," L. In this figure, the product is six. There are five sets of points as noted. Each set of points is joined by line segments and are associated with a fixed input signal-to-noise ration $(SNR)_i$. The relative positions of these curves will remain the same for other products of N_B and L. This is clear from Eq. 38, which indicates that for the same N_B and $(SNR)_i$, $(SNR)_L$ is directly proportional to the square root of L. As an example, for a product of eight, the curves in Fig. 3 will all be shifted upward by a fixed amount of $\sqrt{8/6}$ or 0.6 db.

From this figure, it is clear that analytical results indicate that for a fixed input data bit-volume and output quantity, resolution requirement, and for a constant input signal-to-noise ratio, image quality improvement is obtained by employing more "looks" with coarsely quantized echo samples than to use the same number of bits to obtain more finely quantized signals.

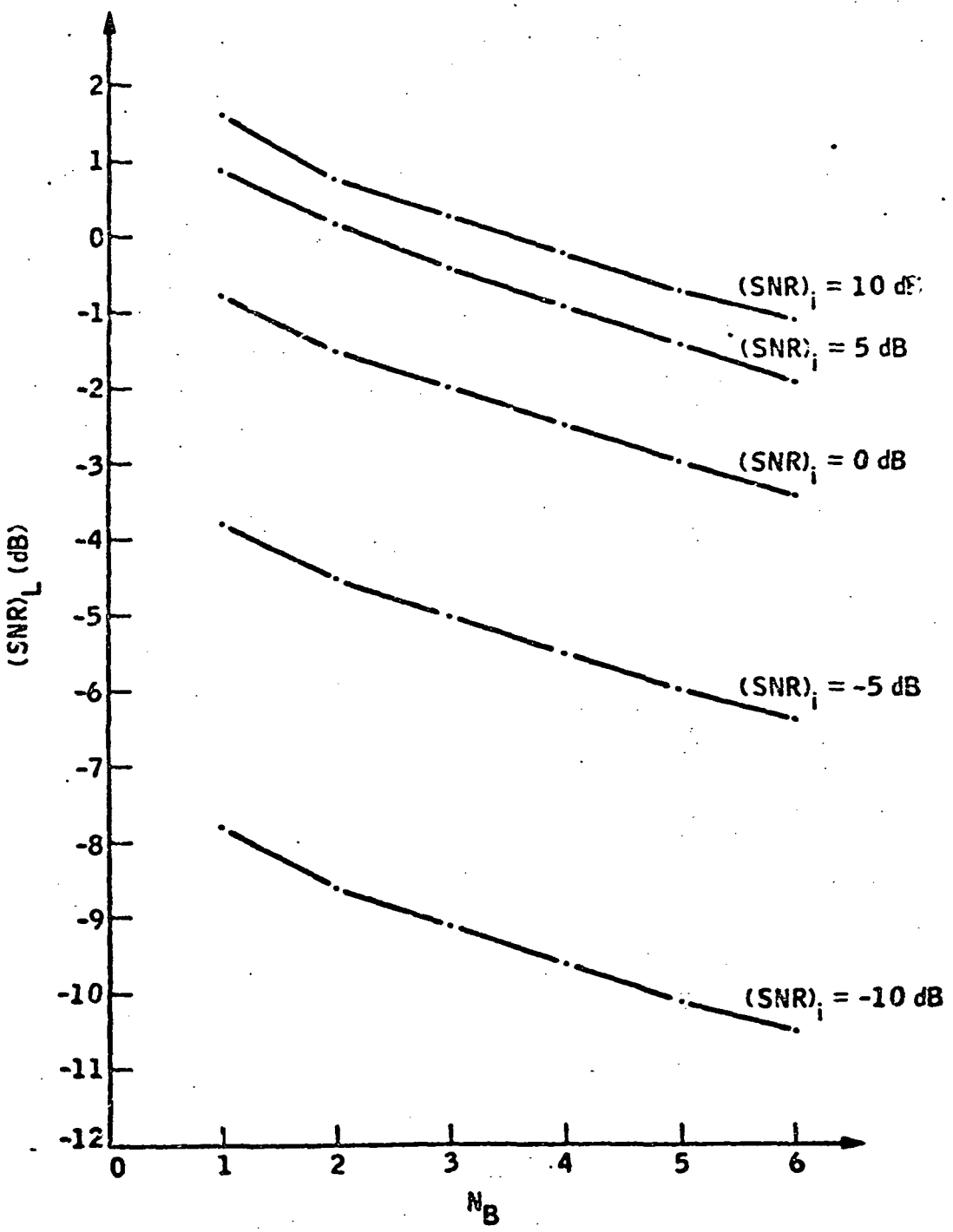

Figure 3 Image Quality for a Fixed Product of Quantization Bits (N_B) and Look Number ($L = 6/N_B$) with Varying Input $(SNR)_i$

IV. SIMULATION RESULTS AND DISCUSSION

A number of simulations were performed using real SAR data to verify the analytical results discussed in the foregoing sections. A digital processing approach was used to reduce SAR signal into images. Two data sets were used in these simulations. One was obtained by scanning and digitizing a piece of an optical signal film. The target area for these data was a mountainous region. The other data set was obtained by directly digitizing the sampled output of a SAR receiver. The scene associated with this data set was a suburban area.

Several different quantization levels and two multiple-look techniques were investigated. One of the multiple look methods (called spatial averaging) involved taking the average of N adjacent pixel values from a one-look "high-resolution" image to produce a "low-resolution" N-look image. The other multiple-look technique (called "spectral averaging") involved taking the average of N independent "low-resolution" images of the same target area. Each independent image was obtained by processing a separate non-overlapping portion (one Nth) of the original signal spectrum.

The results of experiments using the spatial averaging technique are shown in Prints 1, 2, and 3. The three prints correspond to quantization of 1, 2, and 6 bits per sample, respectively. There are three images in each print which are labeled as 1-look, 2-look, and 4-look images respectively. Linear quantization was used for the case of 6 bits per sample quantization, and the minimum distortion quantization scheme was used for the 2 and 1 bit cases. To facilitate direct comparison, each of the three images in each print contains the same

number of pixels. To achieve this in images involving fewer than 4 looks, a uniformly spaced subset of pixels was extracted from the "high resolution" single-look image. Since the speckles are independent from pixel to pixel, this technique does not change the visual quality of the resultant images. The pixel extraction and pixel averaging process for the three different look numbers (1, 2, and 4) is illustrated below

1-look $X = A$

2-look $X = (A+C)/2$

4-look $X = (A+B+C+D)/4$

The results obtained from the "spectral averaging" multiple look approach are shown in Prints 4 to 6. These three prints correspond to 1, 2, and 6 quantization bits, respectively. As in the previous case, the three images labeled (a), (b), and (c) in each print correspond to 1, 2, and 4 look images, respectively. In each print of Prints 4, 5, and 6, the independent single look images were processed by utilizing a non-overlapped portion--one quarter--of the azimuth bandwidth of the corresponding "high resolution" image. One of the four independently processed images was chosen for display as the single look image in each print. The pixels of this single-look image were averaged with those of a second one-look image to produce a two-look image. And finally, the corresponding pixels of all four single-look images were averaged to create a four look image. With

the multiple-look images so arranged on the prints, the effect of speckle noise reduction can readily be observed.

From these results, we note as expected that image quality improves with the increasing of multiple looks and quantization bits. Qualitatively we also notice that the quality of the 2-bit,2-look images appears to be better than that of the 6-bit, 1-look image. This agrees with the analytical results which indicate that in a bit rate limited application, use of fewer bits to obtain more looks is a more effective way to improve image quality than to employ more bits per SAR signal sample.

Notice that the analytical results were derived based on the assumption that the targets being imaged were homogeneous. In a case where the targets do not exhibit this property, the results can be different. The effect is especially noticeable in the extreme case of 1-bit per sample, which is equivalent to applying hard limiting to the baseband I,Q signals. In the one-bit-per-sample images, one can notice the false features in the upper right corners. One can also notice that these false features disappear as the number of quantization levels is increased.

The simulation results also indicate that the two multiple look techniques produce nearly identical results. The choice between these two techniques may heavily depend upon the feasibility of implementation related to each particular SAR data processor.

Image (a) of Print 7 is an optically processed image produced from the corresponding part of the original signal film. By comparing image 7(a) with images in Prints 1 through 6, one can obtain assurance of the integrity of the digital processing technique used in the simulations. This image and the digitally processed images used only a small section of

the swath of the original signal film. An image was also produced from the whole swath using optical processing. Image (b) of Print 7 is a reduced scale rendition of that result. The part of the scene presented in the previous images is located in the upper left part of this image. The speckle in the SAR images is clearly visible in all the full-scale images on Prints 1 through 7.

The experimental results obtained using the second data set will be reported here. The original data were in the form of 6 bit samples of both the inphase and quadrature components of the receiver output. One of the investigations performed with this data set was concerned with the effect of additive noise on the resultant image quality. Different amounts of normally distributed random noises were added to the original signal data. The noise contaminated data were then quantized and processed to produce single-look images. The spatial averaging technique mentioned previously was then used to produce "low-resolution" multiple look images.

The resultant images are presented in Prints 8 to 10. These three prints correspond to three different values for the number of quantization bits per signal sample. They are 1, 2 and 6 bits, respectively, for Prints 8, 9, and 10. On each print there are 12 images. The three columns from left to right correspond to 1, 2, and 4-look images. The four rows of images in each print are associated with four different noise conditions. From top to bottom, the amount of noise added to the original have variances of 0, $0.32\sigma_s^2$, σ_s^2, and $3.2\,\sigma_s^2$, respectively, where σ_s^2 is the variance of the original signal. If it is assumed the original signal contained no additive noise, the three non-zero noise variances correspond to input SNR of 5 db, 0db, and -5 db, respectively.

It can be observed that the image quality improves as either the input signal-to-noise or the multiple-look numbers are increased. Reducing the number of quantization bits does degrade the image quality as indicated in the analysis, but the effect is hardly visible in the resultant images. Also, no serious degradation due to "false features" is visible in the images produced with hard limiting (i.e., one bit quantization) of signal samples. This is attributed to the fact that high contrast features are uniformly distributed in the area being imaged. For such homogeneous targets, the effect of hard limiting becomes less noticeable than other cases associated with non-homogeneous targets. This phenomenon is discussed in Ref. [6] [18]. It can also be observed that image quality appears to degrade substantially as the additional input SNR changes from 0 db to -5 db. This observation generally agrees with the analytical results in Fig. 2, which indicates that image quality is a weak function of the input SNR for values in the region from 0 db to 5 db. Above 5 db, the image quality is almost unaffected by changes in input SNR.

V. CONCLUSION

The analytical results in this study were very well supported by the experimental results. It was concluded from this study that Rayleigh target speckles and integrated sidelobes can often be the key factors in determining the quality of synthetic aperture radar images. The degradation in image quality due to thermal noise in the SAR receiver becomes significant only if the input signal-to-noise ratios are well below 5 db. It was also concluded that in a limited data rate (or volume) application involving homogeneous targets better image quality is obtained by employing more "looks" with coarsely quantized echo samples than by using the

same number of bits to obtain more finely quantized echo signal samples.

It appears that substantial SAR system performance improvements can be achieved by applying the results of this study in future system design.

ACKNOWLEDGEMENTS

The author wishes to thank R. G. Piereson for his many thoughtful suggestions made in the course of this work. He also wishes to thank Dr. S. Butman and Dr. R. G. Lipes for their helpful comments, and A. J. Spear, E. E. Hilbert, R. Jordan, and A. Laderman for their encouragement.

REFERENCES

[1] E.N. Leith, "Quasi-Holographic Techniques in the Microwave Region," IEEE Proc., Vol. 59, No. 9, pp. 1305-1318, Sept. 1971.

[2] R.O. Harger, Synthetic Aperture Radar Systems, Theory and Design. New York: Academic Press, 1970.

[3] W.E. Brown, Jr., C. Elachi, R.L. Jordan, A. Laderman, and T.W. Thompson, Planetary Imaging Radar Study, pp. 4.15 - 4.23, TR701-145, Jet Propulsion Laboratory, Caltech, June, 1972 (JPL internal document).

[4] J.C. Kirk, Jr., "A Discussion of Digital Processing in Synthetic Aperture Radar," IEEE Transaction on Aerospace and Electronic Systems, Vol. AES-11, No. 3, pp. 326-337, May 1975.

[5] R.G. Lipes and S.A. Butman, "Bandwidth Compression of Synthetic Aperture Radar Imagery By Quantization of Raw Radar Data," Proceedings of the SPIE, Vol. 119, pp. 107-114, August, 1977.

[6] B.D. Steinberg, "Hard-Limiting in Synthetic Aperture Signal Processing," IEEE Trans. on Aerospace and Electronic Systems, Vol. AES-11, No. 4, pp. 556-561, July 1975.

[7] A.D. Goldfinger, Distortion Effect in Phase-Coded Radar with Digital Signal Processing, Technical Memorandum TG 1228, Applied Physics Laboratory, John Hopkins University, Nov. 1973.

[8] A. A. Friesem and J.S. Zelenka, "Effects of Film Nonlinearities in Holography," Appl. Opt., Vol. 6,No. 10, pp. 1755-1759, Oct. 1967.

[9] A.R. Sass, "Binary-Intensity Holograms," J. Opt. Soc. Am., Vol. 61, No. 7, pp. 910-915, July, 1971.

[10] J.W. Goodman and G.R. Knight, "Effects of Film Nonlinearities on Wavefront-Reconstruction Images of Diffuse Objects," J. Opt. Soc. Am., Vol. 58, No. 9, pp. 1276-1283, Sept. 1968.

[11] R. Gerchberg, Synthetic Aperture Radar and Digital Processing, TR 177-10, Center for Research, Inc., U. of Kansas, Lawrence, Kansas, Sept. 1970.

[12] R.L. Mitchell, "Models of Extended Targets and their Coherent Radar Images," IEEE Proc. Vol. 62, No. 6, pp. 754-758, June 1974.

[13] N. George, "Speckle," Optics News, pp. 14-22, January 1976.

[14] R.H. Mitchel, SAR Image Quality Analysis Model, Ph.D. Dissertation, U. of Michigan, Ann Arbor, Michigan, 1974.

[15] T.T. Taylor, "Design of Line-Source Antennas for Narrow Bandwidth and Low Side Lobes," IRE Trans. Antennas and Propagations, pp. 16-pp. 28, Jan. 1955.

[16] M.I. Skolnik, Editor-in-Chief, Radar Handbook, Section 20-7, New York, McGraw-Hill, 1970.

[17] J. Max, "Quantizing for Minimum Distortion," IRE Trans. on Information Theory, pp. 7-12, March 1960.

[18] C. Wu, "The Effect of Hard-Limiting on SAR Images," to be published.

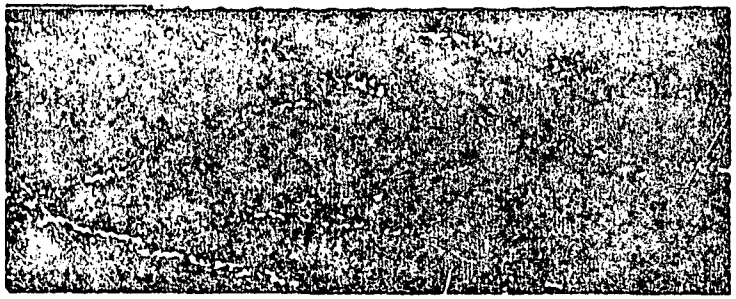

(a) 1-Look

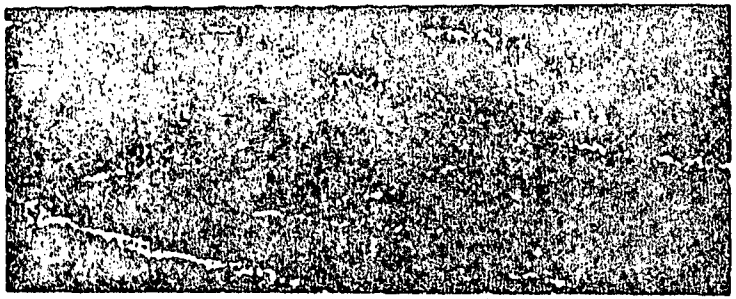

(b) 2-Look

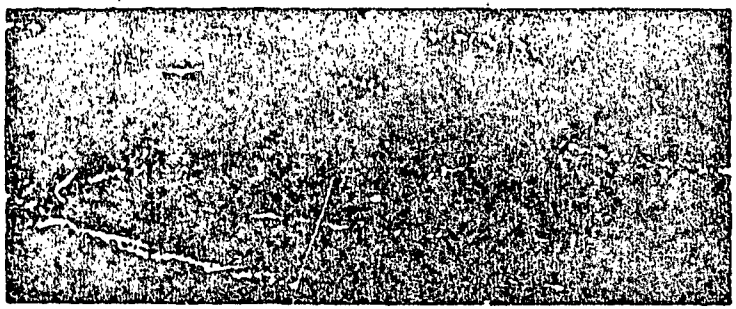

(c) 4-Look

Print 1 SAR Images of One-bit Quantization with Spatial Averaging (1, 2, and 4-Look)

(a) 1-Look

(b) 2-Look

(c) 4-Look

Print 2 SAR Images of Two-bit Quantization with Spatial Averaging (1, 2, and 4-Look)

(a) 1-Look

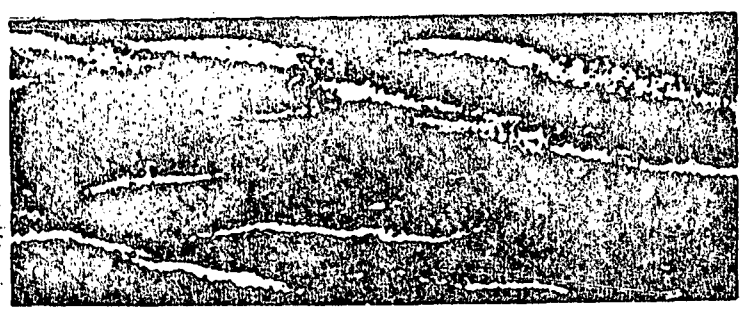

(b) 2-Look

(c) 4-Look

Print 3 SAR Images of Six-bit Quantization with Spatial Averaging (1, 2, and 4-Look)

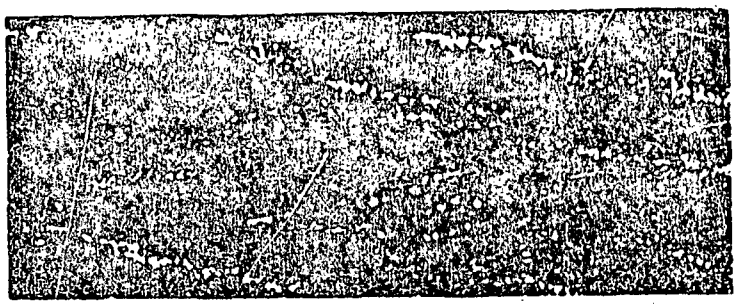

(a) 1-Look

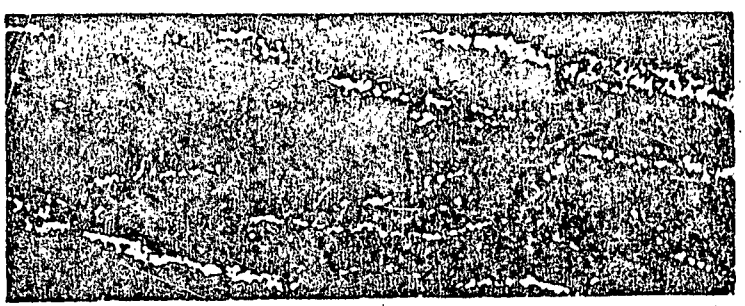

(b) 2-Look

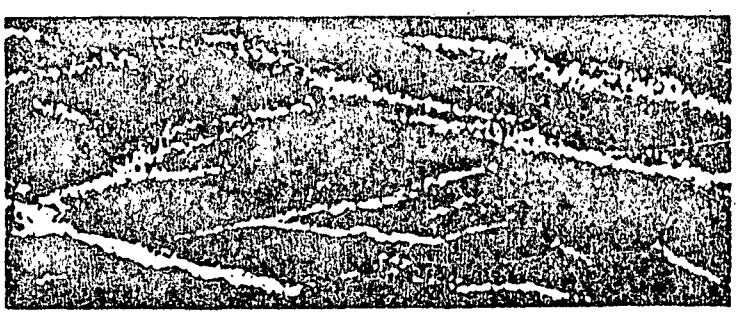

(c) 4-Look

Print 4 SAR Images of One-bit Quantization with Spectral Averaging (1, 2, and 4-Look)

(a) 1-Look

(b) 2-Look

(c) 4-Look

Print 5 SAR Images of Two-bit Quantization with Spectral Averaging (1, 2, and 4-Look

(a) 1-Look

(b) 2-Look

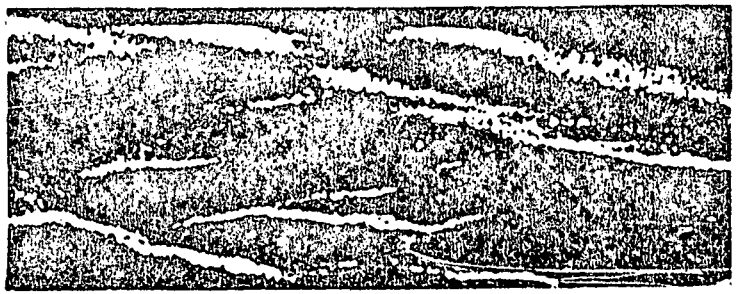

(c) 4-Look

Print 6 SAR Images of Six-bit Quantization with Spectral Averaging (1, 2, and 4-Look)

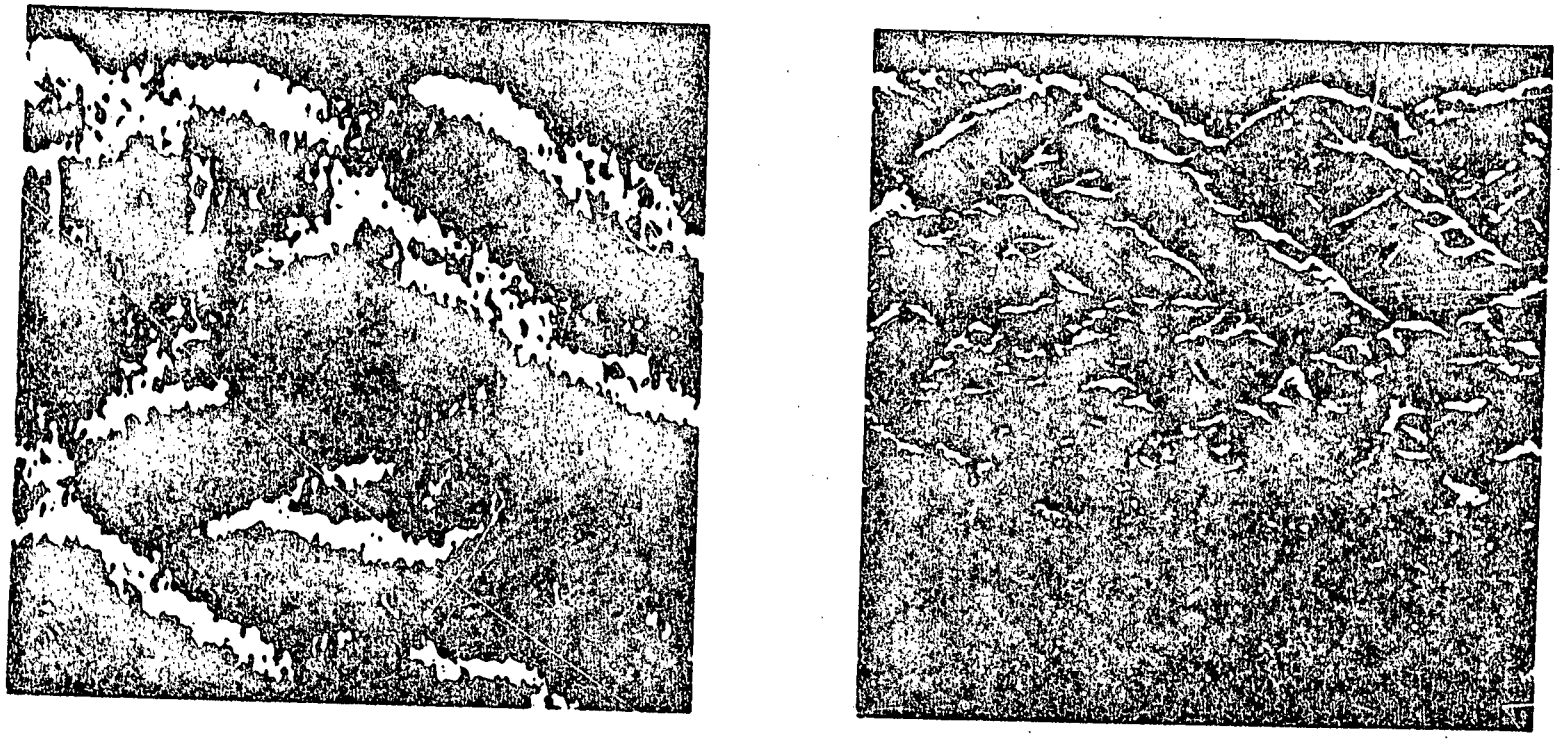

(a) (b)

Print 7 A SAR Image over a Mountainous Area

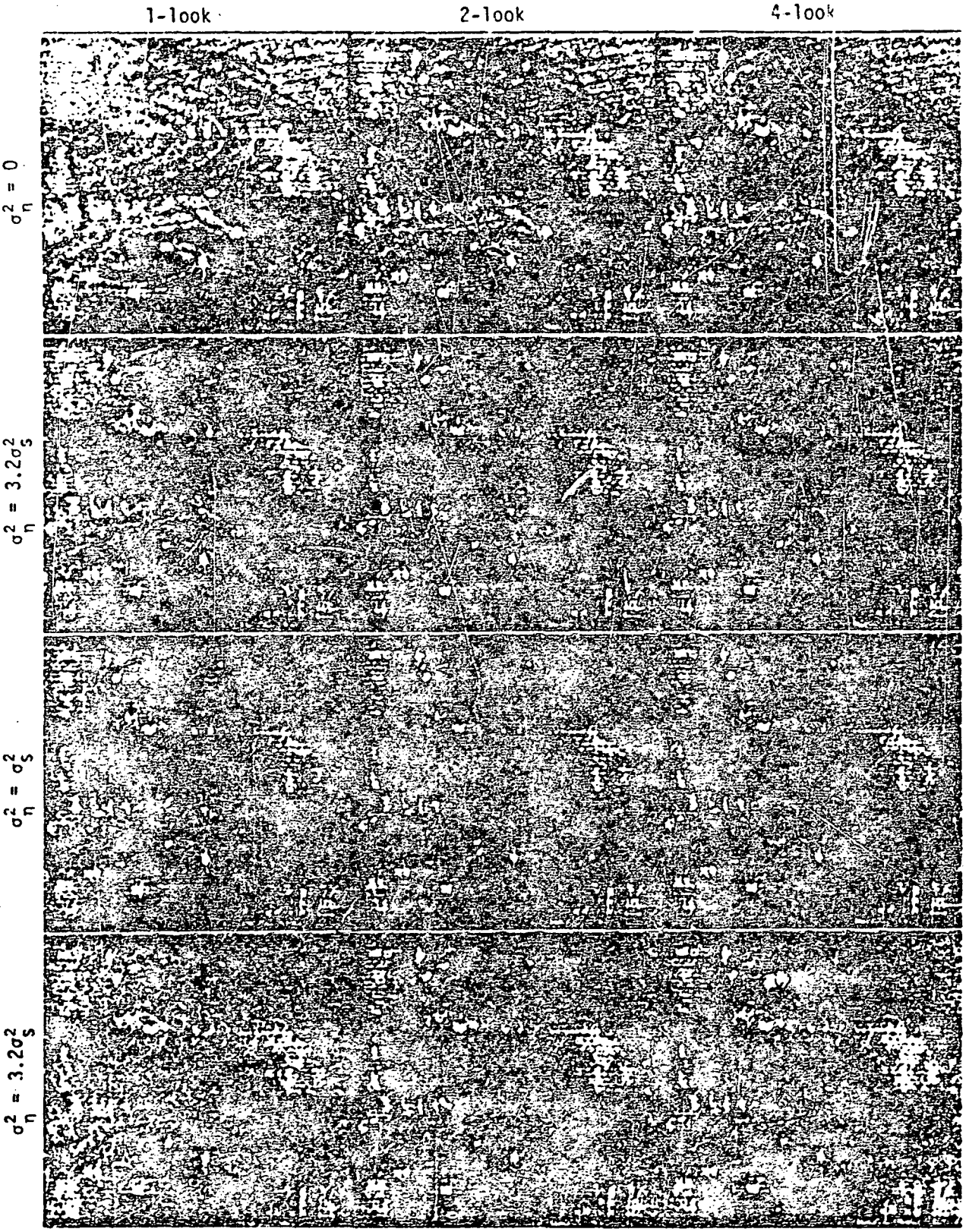

Print 8 Effect of One-bit Quantization with Varying Input Signal-to-Noise Ratio and Look Number on SAR Images

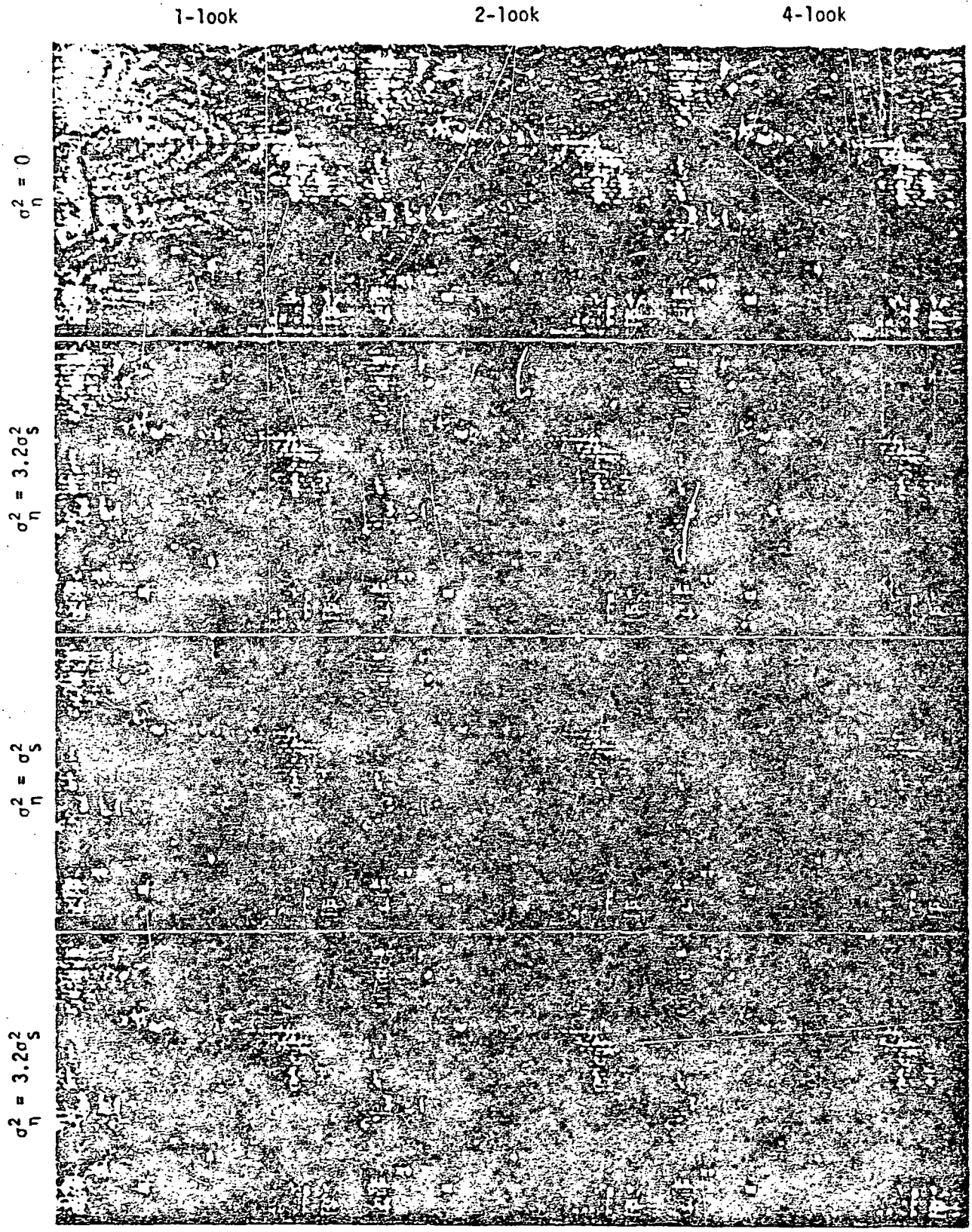

Print 9 Effect of Two-bit Quantization with Varying Input Signal-to-Noise Ratio and Look Number on SAR Images

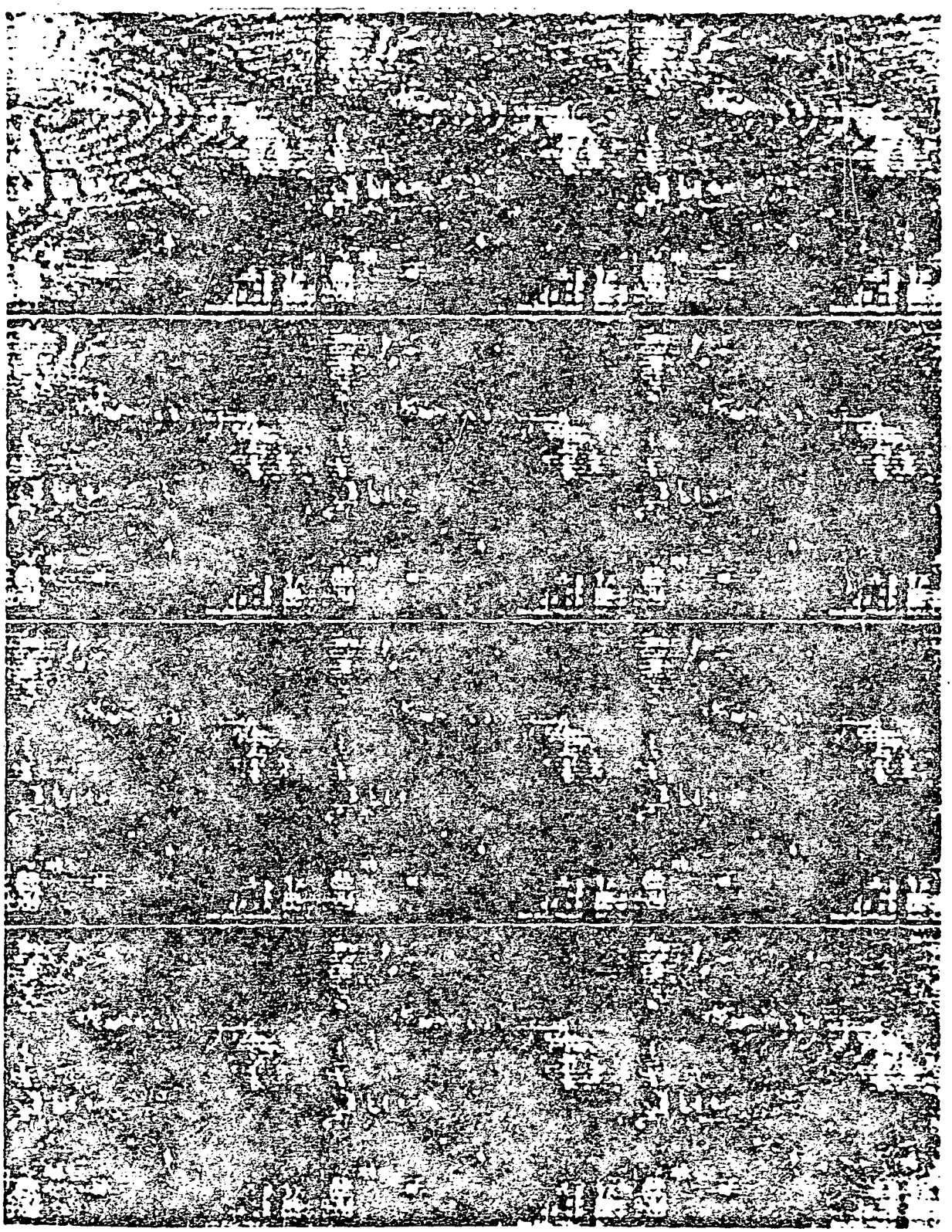

Print 10 Effect of Six-bit Quantization with Varying Input Signal-to-Noise Ratio and Look Number on SAR Images

END

DATE

FILMED

SEP 25 1978